Equilibrium solutions of MHD equations for GAMs in the edge tokamak plasma

R.V. Shurygin[1], A.V. Melnikov[1]

[1] NRC 'Kurchatov Institute', Moscow, Russia

E-mail contact of main author: regulxx@rambler.ru

Abstract. Numerical calculations of nonlinear MHD equations in frames of reduced two-fluid Braginskij equations for geodesic acoustic modes (GAMs) with n = 0, m = 0, +1, -1 in high-collisional edge tokamak plasma were performed. It was shown that account of parallel dissipation (finite conductivity σ//) allows us to obtain the steady state equilibrium solutions for GAMs. The obtained two-dimensional equilibrium includes the poloidal rotation velocity and the equilibrium electric potential, which value is close to the well-known Pfirsh-Schlüter potential. The main role in formation of the equilibrium poloidal rotation plays two forces: the Stringer-Winsor force and the neoclassical force, linked with the parallel viscosity. Obtained solutions show that maximal values of GAM are located near the maximum of pressure gradient. On the radial profile of electric field the parabolic well (E<0) is seen.

1. Introduction

Clearly developed interest both theorists and experimenters to investigation of MHD geodesic acoustic modes (GAMs) with toroidal and poloidal numbers n=0, m=0, ±1 is determined by fact that poloidal flows formed by these modes sufficiently influence to the turbulent activity in the tokamak plasma. Apart the Reynolds force, the Stringer-Winsor force driven by the GA mode of total pressure plays important role in the plasma poloidal rotation. Traditional approach to GAM investigation consists of deriving and following analysis of dispersion relation, obtaining from linearized set of two-fluids Braginskii equations.

The spectral approach allows us to obtain the spectrum of oscillations either in the local approximation $\omega=f(r)$, or as array of eigenvalues after solution of the differential equations. However, this approach becomes not quite adequate to experiment owing to rather arbitrary choice of equilibrium (finding of which may be separate problem) and to absence both of nonlinear terms and physically meaningful boundary conditions. In recent years the solutions of nonlinear reduced two-fluids Braginskii equations are used for GAM investigations [1-4]. It is well known that solution of such system of MHD equations even in its simplest form (Hasegawa-Wakatani model [5]) shows the turbulent properties. The turbulence is a consequence of three-dimensionality of the problem ($\partial/r\partial\theta$, $\partial/R\partial\phi$) and nonlinear interaction of modes with different m and in the convection term, which looks like the Poisson brackets $\{A, B\}=1/r[dA/dr \cdot dB/d\theta - dB/dr \cdot dA/d\theta]$. Implementation of solution of this MHD set is possible only with a numerical code, so it is a nontrivial problem, which demands considerable efforts.

However, we may considerably simplify this MHD set, if we take into account that geodesic modes are modes with n=0, m=0,±1. In the presented paper this simplification is linked with account of these three modes and omitting of modes with $m \geq 2$. Thus we study the evolution

of MHD system containing the geodesic modes only. The MHD equations are solved by the numerical simulation.
Calculations have show that in the considered set of equations the turbulence is absent, and for $t \to \infty$ the solutions approach to the steady values. At modest electron temperatures (~50 eV) at initial stage, during the time range 0–800 μs, we see the GAM oscillations with frequencies ω≈10.4 kHz, while the theoretical value is Ω_{GAM} = 8.8 kHz. Then the oscillations are damped and approaches to the equilibrium value.

2. Basic equations

We use two-field $\{\varphi, p_e\}$ set of reduced two-fluid Braginskii equations, which describes behavior of GAMs with n=0, m=0,±1 [1]. We consider the approximation $p_i = \tau \cdot p_e$ with permanent density n_0=const:

$$\frac{n_0 mc^2}{B^2}\left(\frac{\partial w}{\partial t} + \mathbf{V_E}\cdot\nabla w\right) = \nabla_\parallel j_\parallel + e\mathbf{Y}\cdot\nabla(p_e + p_i) + \frac{n_0 mc^2}{B^2}\left(\mu\Delta_\perp w - \frac{1}{r}\frac{d}{dr} rF_{NEO}\right), \quad (1)$$

$$\frac{\partial p_e}{\partial t} + \mathbf{V_E}\cdot\nabla p_e = \frac{5}{3}\frac{p_e}{en_0}\nabla_\parallel j_\parallel + \frac{j_\parallel}{en_0}\nabla_\parallel p_e + \frac{5}{3}\mathbf{Y}\cdot\{\nabla(p_e T_e) - ep_e\nabla\varphi\} + \chi_{\parallel e}\cdot\nabla_\parallel^2 p_e + \chi_{e\perp}\Delta_\perp p_e \quad (2)$$

where

$$w = \nabla_\perp{}^2\varphi, \qquad j_\parallel = \sigma_\parallel\left(\frac{\nabla_\parallel p_e}{en_0} - \nabla_\parallel\varphi\right), \qquad \nabla_\parallel = \frac{1}{qR_0}\frac{\partial}{\partial\theta},$$

$$\sigma_\parallel = \frac{e^2 n_0}{0.51 m_e \nu_{ei}}, \qquad \chi_{\parallel e} = \frac{2\cdot 3.16\, p_e}{3 m_e \nu_{ei} n_0}, \qquad \mathbf{Y} = \frac{2c\nabla B}{eB^2}, \qquad \mathbf{V}_E = \frac{c}{B_0}[\mathbf{b}\times\nabla\varphi].$$

The set (1–2) may be rewritten in dimensionless form using the transformation of variables $n\to n(d/L_0)/n_{19}$, $p\to p(d/L_0)^2/n_{19}T_*$, $\varphi\to\varphi/\varphi_*$, $r\to r/L_0$, $t\to t/t_*$, where n_{19} is density in 10^{19} m^{-3},

$t_* = \frac{1}{C_S}\sqrt{\frac{R_0 d}{2}}$, $\varphi_* = \frac{B_0}{c}\frac{L_0^2}{t_*}$, d is a width of the calculated layer, T_*=100 eV.

$$L_0 = q\sqrt{\frac{0.51\rho_S R_0 \nu_{ei0}}{\omega_{ce}}}\left(\frac{2R_0}{d}\right)^{1/4}, \quad C_S = \sqrt{\frac{T_*}{m_i}}, \quad \rho_S = \frac{C_S}{\omega_{ci}}, \quad \omega_{ce,i} = \frac{eB_0}{m_{e,i}c}, \quad \omega_* = \frac{1}{t_*}.$$

To obtain the set of nonlinear MHD equations, which describes electrostatic GAMs in each of field variables $\{w, \varphi, p_e\}$, we use the decomposition

$$f(r,\theta,t) = f_0(r,t) + f_S(r,t)\cdot\sin\theta + f_C(r,t)\cdot\cos\theta.$$

As a result, we obtain the set of 6 nonlinear differential equations for variables $\{f_i\}=\{w_0, w_S, w_C, p_0, p_S, p_C\}$ in the following form:

$$\frac{\partial w_0}{\partial t}+\frac{1}{r}\frac{d}{dr}r\Pi_0=-\frac{1+\tau}{2n_0}\frac{dp_S}{dr}+\frac{\mu}{r}\frac{d}{dr}r\frac{dw_0}{dr}-\frac{1}{r}\frac{d}{dr}rF_{NEO}$$
$$\frac{\partial w_S}{\partial t}+\Pi_S=-\frac{1+\tau}{n_0}\frac{dp_0}{dr}-\frac{H_S}{\nu}+\frac{\mu}{r}\frac{d}{dr}r\frac{dw_S}{dr}$$
$$\frac{\partial w_C}{\partial t}+\Pi_C=-\frac{H_C}{\nu}+\frac{\mu}{r}\frac{d}{dr}r\frac{dw_C}{dr}$$

$$\frac{\partial p_0}{\partial t}+\frac{1}{r}\frac{d}{dr}rQ_0=-D_0+\frac{5}{3}g\psi_0+\frac{\chi}{r}\frac{d}{dr}r\frac{dp_0}{dr}$$
$$\frac{\partial p_S}{\partial t}+Q_S=-D_S+\frac{5}{3}g\psi_S+\frac{\chi}{r}\frac{d}{dr}r\frac{dp_S}{dr}$$
$$\frac{\partial p_C}{\partial t}+Q_C=-D_C+\frac{\chi}{r}\frac{d}{dr}r\frac{dp_C}{dr} \qquad (3)$$
$$D_0=\frac{\sigma_1}{3}[p_SH_S+p_CH_C]+\frac{\sigma_2}{2}[p_S^2+p_C^2]$$
$$D_S=\frac{5}{3}\sigma_1p_0H_S+\sigma_2p_0p_S,\quad D_C=\frac{5}{3}\sigma_1p_0H_C+\sigma_2p_0p_C$$

$$H_{S,C}=\frac{\alpha}{n_0}p_{S,C}-\varphi_{S,C},\quad \Pi_0=\frac{1}{2r}[\varphi_Cw_S-\varphi_Sw_C],\quad \Pi_{S,C}=\mp\frac{1}{r}[\varphi_0'w_{C,S}-\varphi_{C,S}w_0']$$

$$\psi_0=\frac{1}{2}[p_SY_0'+p_0Y_S'-\xi(T_Sp_0'+T_0p_S')],\quad Y=\varphi-\xi T$$
$$\psi_S=p_0Y_0'-\xi p_0'T_0$$
$$Q_0=\frac{1}{2r}[\varphi_Cp_S-\varphi_Sp_C],\quad Q_{S,C}=\mp\frac{1}{r}[\varphi_0'p_{C,S}-\varphi_{C,S}p_0']$$

The set (3) is solved together with equations $\frac{1}{r}\frac{d}{dr}r\frac{d\varphi_{S,C}}{dr}-\frac{\varphi_{S,C}}{r^2}=w_{S,C}$.

From equation for $\frac{\partial w_0}{\partial t}$ with condition n_0=const and taking into account that $w_0=\frac{1}{r}\frac{d}{dr}rV_{POL}$ we obtain equation for the poloidal ion velocity V_{POL}:

$$\frac{\partial V_{POL}}{\partial t}=F_{RE}+F_{SW}+F_{NEO}+F_\mu$$
$$\Pi=\frac{1}{2r}[\varphi_CW_S-\varphi_SW_C],\qquad F_{NEO}=-\mu_{NEO}\cdot[V_{POL}-V_{NEO}] \qquad (4)$$

Equation (4) shows that poloidal ion velocity is determined by action of four forces: Reynolds stresses F_{RE}=-Π_0, the Stringer-Winsor force F_{SW}=-(1 + τ)p_S/(2n_0), the neoclassical force F_{NEO} and viscous force F_μ=μ/r d/dr(r dV_{POL}/dr). For variables μ_{NEO} and V_{NEO} we use expressions from [6]. The value $V_{POL}(r, t)$ (zonal flow) increases with growth of the electron temperature in the edge region (Figure 2). The electric field is calculated from the relation:

$$\frac{c}{B_0}\frac{d\varphi_0}{dr} = V_{POL} - V_{Di}\,, \tag{5}$$

where V_{Di}=c(dp_i/dr)/enB_0 is the diamagnetic ion velocity. The potential is calculated as follows:

$$\varphi_0(r,t) = \frac{B_0}{c}\int_r^a [V_{POL} - V_{Di}]dr \tag{6}$$

with the boundary condition $\varphi_0(a) = 0$, $r_1 < r < a$. Analysis shows that the effect of diamagnetic velocity in equation (3.1) may be not small, and it should be included in calculations of the electric field $E(r, t)$.

3. Numerical results

Numerical calculations were performed for the edge region (r_0 = 0.24 m < r < a = 0.3 m, -π<θ<π, d = a - r_0) of the T-10 tokamak with following parameters: R=1.5 m, d=0.06 m, B=1.8 T, q_{res}=3-4, $n_0(r_0)$ =1.0–2.0, $n_0(a)$=0.2 (density in 10^{19} m^3), $T_{e0}(r_0)$=50 –250 eV, $T_{e0}(a)$=20 eV, T_{i0}=τ T_{e0}, τ=0.8.

The numerical simulations of evolution of the set (3) were performed for different electron temperatures T_{be} = $T_{e0}(r_0)$ = 50, 150 and 250 eV, and $n(r_0)$ = 1.0. Calculations have show that the steady state established as faster, as larger the electron temperature of the layer (*FIG.* 1). The poloidal ion velocity and corresponding value of the radial electric field are also increasing with growth of the temperature, as it is seen in Figures 2–3. The physical reason of approach to the steady state is establishment of balance in (1-2) between terms with longitudinal dissipation $\sigma_{//} \sim T_e^{3/2}$ and terms, which determine the growing solutions ~dp/dr. Note that known analytical solution for the Pfirsh-Schlüter potential, obtained from the simplified expression

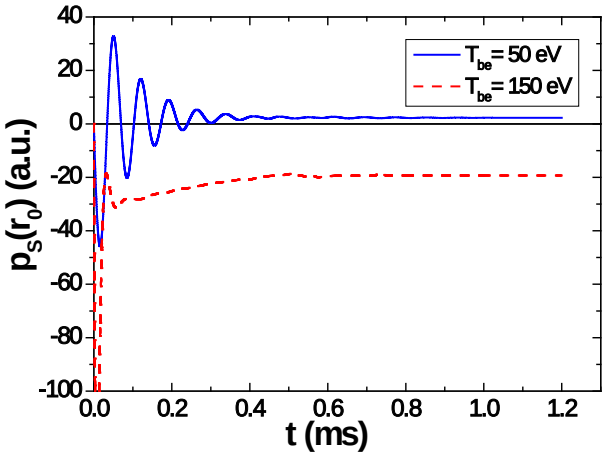

FIG. 1. The time evolution of the sine component of pressure p_S for electron temperatures T_{be}=50 and 150 eV.

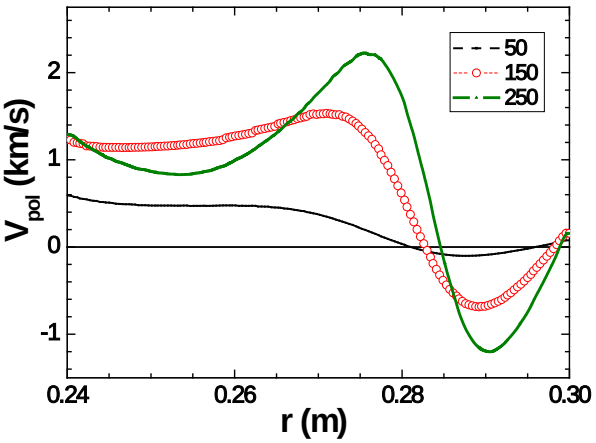

FIG. 2. Radial profiles of the poloidal velocity for T_{be}=50, 150 and 250 eV.

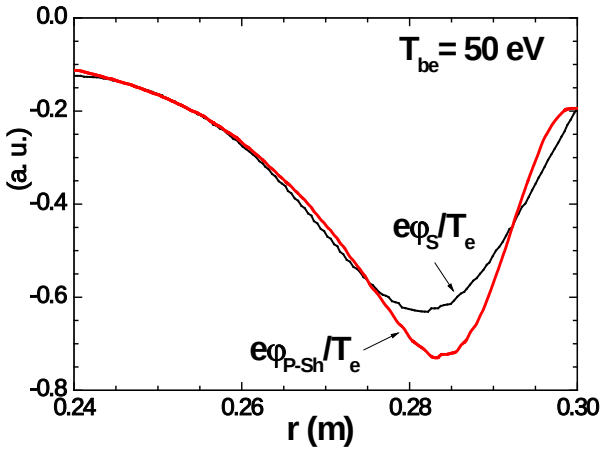

FIG. 3. Radial profiles of the sine component of potential and the Pfirsh-Schlüter potential for T_{be}=50 eV.

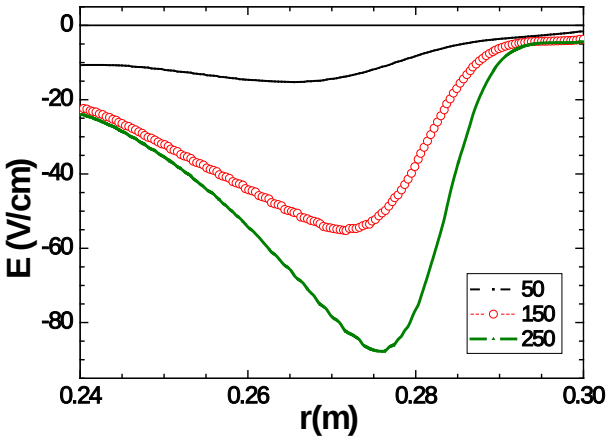

FIG. 4. Radial profiles of the electric field for T_{be}=50, 150 and 250 eV.

$$\mathrm{div}(\mathbf{j}_\parallel + \mathbf{j}_\perp) \approx 0, \quad \frac{1}{qR_0}\frac{\partial j_\parallel}{\partial \theta} = -\mathrm{div}\frac{c\mathbf{B}\times\nabla p}{B^2} \approx \frac{2c\mathbf{b}\times\nabla B}{B^2}\nabla p$$

$$j_\parallel = -\frac{\sigma_\parallel(r)}{qR_0}\frac{\partial \varphi}{\partial \theta}, \quad B \approx B_0\left(1-\frac{r}{R_0}\cos\theta\right)$$

has the form

$$\varphi(r,\theta) = \varphi_{P-Sh}(r)\sin\theta, \quad \varphi_{P-Sh}(r) \approx \frac{2q^2R_0c}{\sigma_\parallel B_0}\frac{dp}{dr}, \qquad (7)$$

and with a good accuracy it coincides with Fourier-sine component, obtained from numerical calculations of the potential

$$\varphi_{NUM}(r,t,\theta) = \varphi_S(r,t)\sin\theta + \varphi_C(r,t)\cos\theta, \quad \varphi_S \approx \varphi_{P\_Sh}$$

The numerical and analytical values of sine component of potential are shown in Figure 3. Obtained solutions show that the maximal values of GAMs are located near the point with maximal value of the pressure gradient. In future, it would be interesting to compare the measured parametric dependencies of the potential on T, n, B_0, q with similar dependencies following from analytical expression (7), and understand, at which degree the potential calculated by (7) agrees with experimental data. Figure 4 shows the radial profile of the field $E(r)$ with the typical parabolic «well», where $E = -d\varphi_0/dr < 0$ that often observed in experiments. Figures 5 and 6 show the radial dependencies of the time-averaged equilibrium values of sine and cosine components of pressure $p_S(r)$ and $p_C(r)$. Figures 7 and 8 show the radial dependencies of zero and sine component of potential $\varphi_0(r)$ and $\varphi_S/T(r)$ correspondingly.

The obtained steady-state solution (at $t \to \infty$) leads to conclusion that GAM oscillations observed in experiment may exist only in the turbulent regime of tokamak, when the energy exchange between GAMs and small-scale turbulent fluctuations with various m and n occurs. In the considered set (3) we use only three modes (m = 0, +1, -1). As a result, in spite of presents of nonlinear terms the turbulence is absent, because they are small; oscillations damped in time and the steady state is established.

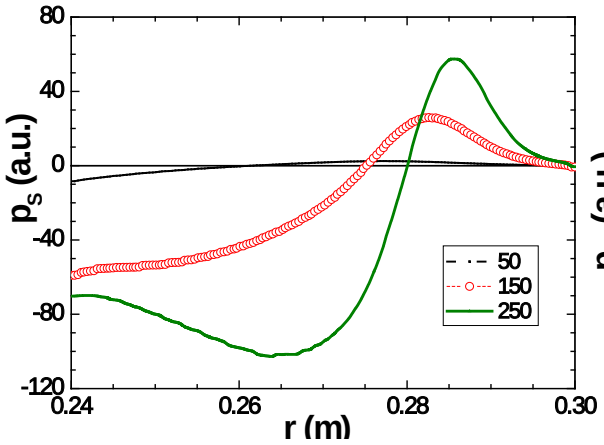

FIG. 5. Radial profiles of sine component of electron pressure p_S for T_{be}=50, 150 and 250 eV.

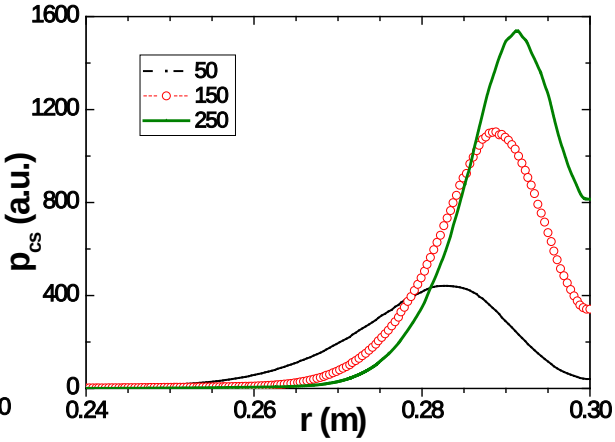

FIG. 6. Radial profiles of cosine component of electron pressure p_{CS} for T_{be}=50, 150 and 250 eV.

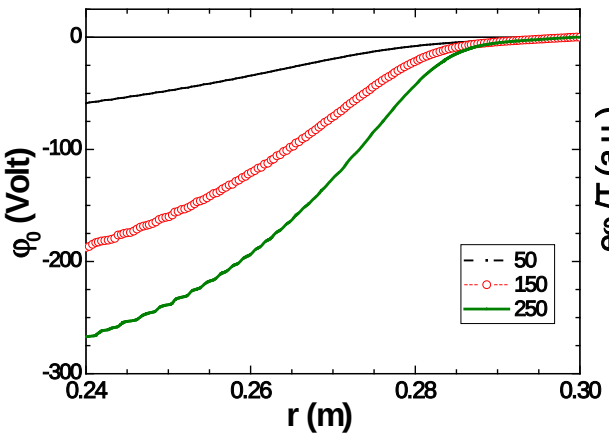

FIG. 7. Radial profiles of zero component of potential for T_{be}=50, 150 and 250 eV.

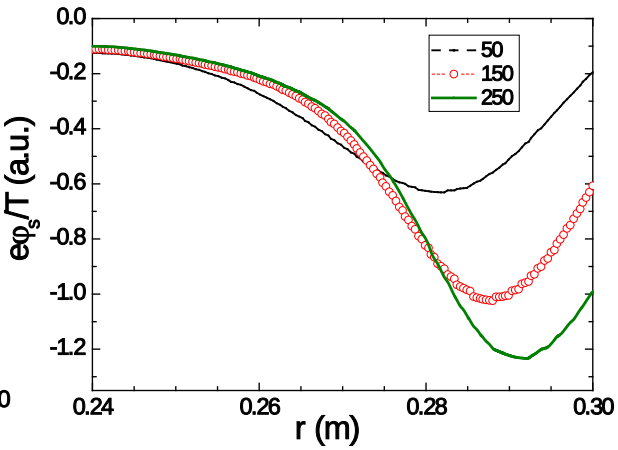

FIG. 8. Radial profiles of sine component of potential for T_{be}=50, 150 and 250 eV.

4. Conclusions

The system of nonlinear MHD equations for geodesic acoustic modes (GAMs) with n=0, m=0, +1, -1 is numerically solved in frames of reduced two-fluid Braginskii model for the high-collisional edge tokamak plasma. It was shown that account of longitudinal dissipation (finite $\sigma_{\|}$) allows us to find the steady-state equilibrium solutions for these modes. Obtained 2D equilibrium includes the poloidal rotation velocity, and the equilibrium electric potential, which is close to the well-known analytical solution – the Pfirsch-Schlüter potential. Existence of analytical expression for the sine component of geodesic potential allows us to compare parametric dependencies of potential on T, n, B_0, and q with experimental measurements. Calculations have shown that the main role in formation of the equilibrium potential rotation velocity play two forces: the Stringer-Winsor force and the neoclassical force linked with the longitudinal viscosity. Obtained solutions show that maximal values of GAMs are located near the point with maximal pressure gradient. On the radial profile of calculated electric field the parabolic "well" (E<0) is seen.

Absence of turbulence in the system may be explained by using three-mode approximation and, as a consequence, smallness of obtained nonlinear terms. As a result, the quadratic nonlinearity cannot form attracting centers (similar to Lorentz attractor) in the phase space, and stochastic solutions occurred due to attractors are not realized.

The work is funded by Russian Science Foundation (project 14-22-00193).

References

[1] SHURYGIN, R.V., MAVRIN, A.A. "Numerical simulation of drift-resistive ballooning turbulence in the presence of the GA mode in the plasma edge tokamak", Plasma Phys. Rep. **36** (2010) 535.

[2] SINGH, R. et al., "Geodesic acoustic modes in a fluid model of tokamak plasma: the effects of finite beta and collisionality", Plasma Phys. Control. Fusion **57** (2015) 125002.

[3] MIKI, K., et al., "Intermittent Transport Associated with the Geodesic Acoustic Mode near the Critical Gradient Regime", Phys. Rev. Lett. **99** (2007) 145003.

[4] MIKI, K., et al., "Dynamics of turbulent transport dominated by the geodesic acoustic mode near the critical gradient regime", Phys. Plasmas **15** (2008) 052309.

[5] SUGAMA, H., et al., "Study of resistive drift and resistive interchange modes in a cylindrical plasma with magnetic shear", Phys. Fluids **31** (1988) 1601.

[6] KIM, Y.B., et al., "Neoclassical poloidal and toroidal rotation in tokamaks", Phys. Fluids B. **3** (1991) 2050.